Investigating the feasibility of channelrhodopsin variants for nanoscale optogenetics

Markus A. Stahlberg
Charu Ramakrishnan
Katrin I. Willig
Edward S. Boyden
Karl Deisseroth
Camin Dean

Investigating the feasibility of channelrhodopsin variants for nanoscale optogenetics

Markus A. Stahlberg,[a] Charu Ramakrishnan,[b] Katrin I. Willig,[c] Edward S. Boyden,[d] Karl Deisseroth,[b] and Camin Dean[a],*

[a]European Neuroscience Institute, Trans-Synaptic Signaling Group, Goettingen, Germany
[b]Stanford University, Howard Hughes Medical Institute, Department of Bioengineering, Department of Psychiatry, CNC Program, Stanford, California, United States
[c]University Medical Center, Center for Nanoscale Microscopy and Molecular Physiology of the Brain, Goettingen, Germany
[d]MIT Media Lab and McGovern Institute, Departments of Brain and Cognitive Science and Biological Engineering, Cambridge, Massachusetts, United States

Abstract. Optogenetics has revolutionized the study of circuit function in the brain, by allowing activation of specific ensembles of neurons by light. However, this technique has not yet been exploited extensively at the subcellular level. Here, we test the feasibility of a focal stimulation approach using stimulated emission depletion/reversible saturable optical fluorescence transitions-like illumination, whereby switchable light-gated channels are focally activated by a laser beam of one wavelength and deactivated by an overlapping donut-shaped beam of a different wavelength, confining activation to a center focal region. This method requires that activated channelrhodopsins are inactivated by overlapping illumination of a distinct wavelength and that photocurrents are large enough to be detected at the nanoscale. In tests of current optogenetic tools, we found that ChR2 C128A/H134R/T159C and CoChR C108S and C108S/D136A—activated with 405-nm light and inactivated by coillumination with 594-nm light—and C1V1 E122T/C167S—activated by 561-nm light and inactivated by 405-nm light—were most promising in terms of highest photocurrents and efficient inactivation with coillumination. Although further engineering of step-function channelrhodopsin variants with higher photoconductances will be required to employ this approach at the nanoscale, our findings provide a framework to guide future development of this technique. © *The Authors. Published by SPIE under a Creative Commons Attribution 4.0 Unported License. Distribution or reproduction of this work in whole or in part requires full attribution of the original publication, including its DOI.* [DOI: 10.1117/1.NPh.6.1.015007]

Keywords: optogenetics; channelrhodopsin; RESOLFT microscopy; STED microscopy.

Paper 18062RR received Oct. 17, 2018; accepted for publication Feb. 5, 2019; published online Feb. 28, 2019.

1 Introduction

Approaches to examine the biological mechanisms underlying synaptic plasticity rely on the artificial stimulation of neurons. Since its discovery, channelrhodopsin 2 (ChR2)—a channel that depolarizes neurons when activated by blue light—and its derivatives have become the dominant technique used to activate or inactivate neurons.[1] So far, the stimulation of neurons using channelrhodopsins has mainly focused on targeting specific cell populations or areas in the brain of rodents.[2,3] But the ability to stimulate subcellular nanodomains using channelrhodopsins[4] has not yet been extensively explored. Such a technique would be particularly advantageous to study aspects of synapse-specificity (where single synapses range in size from 0.04 μm^{25} to ~0.1 μm^3 for a dendritic spine) or the features of subsynaptic nanodomains.

Several attempts have been made to decrease the area of activation of channelrhodopsins. Spatially controlled stimulation of postsynaptic sites has been achieved by optogenetic stimulation of the presynaptic neuron,[6] for example. An activated area less than 30 μm in diameter was achieved by focused laser beams with reduced laser power,[7] and two-photon stimulation with 920-nm light has been used to evoke action potentials in individual cells.[8–10] However, so far, no technique exists that confines stimulation of light-gated channels to defined microscale—or nanoscale—subcellular regions. Focal activation of

neurons could, in principle, be achieved using a stimulated emission depletion (STED)/reversible saturable optical fluorescence transitions (RESOLFT)-inspired illumination approach in which a focal light beam of one wavelength is used to activate channels, and a surrounding overlapping donut beam of another wavelength inactivates them. We tested such an approach by making use of mutations in light-gated channels that slow the photocycle, making it easier to control their switching between active and inactive states in response to two different wavelengths of light.

The photocycle of ChR2 has been intensively studied.[11–14] When ChR2 is illuminated with blue light, it undergoes a conformational change from its dark-adapted closed state (D470), through two nonconducting intermediate states (P500 and P390), and enters the open-channel state (P520). Subsequently, it passes through several intermediate states, until it finally reaches its dark-adapted closed state again and the cycle can be repeated. Interestingly, the P390 intermediate state and the P520 open state are sensitive to UV light (~390 nm) and green light (~520 nm), respectively, which mediate a direct transition to the closed-channel state (D470).[14] ChR2 channels that possess a mutation at residue C128—a conserved amino acid that interacts with the all-trans retinal Schiff base chromophore—have delayed inactivation and a prolonged open state following blue light activation, which can be converted directly to the closed state by green light, creating a so-called "step function" opsin.[15] The ChR2 C128S, C128T, and C128A step-function opsin mutants possess long open-channel states. These channels

*Address all correspondence to Camin Dean, E-mail: c.dean@eni-g.de

can be efficiently closed by exposure to a second closing wavelength (and opened again by an activating wavelength). However, the mutations that cause channels to close in response to a second wavelength of light often result in a reduction in photocurrent.[15]

Focal activation of neurons by activating channelrhodopsins with one wavelength and inactivating them with an overlapping donut of another wavelength requires that channels have a high enough photocurrent to detect focal (micro- or nanoscale) activation and be efficiently inactivated by overlapping illumination of a distinct wavelength. Here, we tested channelrhodopsin variants for these properties.

2 Results

Focal stimulation of channelrhodopsins requires that activated channels remain relatively immobile in cell membranes. We therefore first tested the diffusion of channelrhodopsins expressed in dissociated hippocampal neurons. STED microscopy images of transfected dissociated hippocampal neurons revealed that ChR2-EYFP was mainly targeted to the plasma membrane of neurons [Fig. 1(a)]. To examine channel diffusion, we performed fluorescence recovery after photobleaching (FRAP) experiments. A 2.5-μm region was illuminated with 488-nm light at 100% laser power for 1 s to bleach ChR2-EYFP in the illuminated region in neuronal processes or cell bodies and imaged for 200 s postbleaching [Fig. 1(b)]. ChR2-EYFP fluorescence in the bleached region recovered partially, with a diffusion coefficient of $3.3 \pm 0.2 \times 10^{-2}$ μm^2/s in processes and $4.7 \pm 0.02 \times 10^{-2}$ μm^2/s in cell bodies, indicating low mobility, such that centrally activated channels would be inactivated by overlapping donut coillumination 500 nm in width or greater, assuming complete inactivation of step function opsin channels within 1 s.[15]

A prerequisite for a potential micro/nanoscale focal illumination approach is that channels (1) have a relatively high photocurrent, to allow detection of focal activation, and (2) can be activated by one wavelength of light and inactivated by simultaneous overlapping illumination with another wavelength. Because high photocurrents and inactivation of channelrhodopsins with a second overlapping wavelength of light is difficult to predict based on structure-function analysis, we tested a broad range of channelrhodopsin variants for these properties. Dissociated hippocampal cultures were transfected with expression constructs of EYFP or mCherry-tagged light-gated ion-channels using calcium phosphate. Channel-specific light-evoked photocurrents were then tested to determine channel activation spectra, conductance, gating kinetics, and the ability to close channels with a second wavelength, using patch-clamp recordings of cells identified by their respective fluorescence. Spontaneous activity was suppressed by application of TTX, APV, CNQX, and gabazine, during recordings from neurons voltage-clamped at −70 mV. For each channel, we measured photocurrents elicited by 405, 488, 561, 594, and 639 nm single wavelength laser illumination. Subsequently, channel inactivation was tested by coillumination with all available laser combinations. Only the wavelength combinations for which effects were observed are shown in subsequent figures.

The first group of tested channels included the ChR2 variants with comparatively fast-photocycles: H134R, T159C, E123T/T159C, and L132C. Fast photocycle channels do not possess a stable open-channel state and will open, close, and reopen in relatively fast succession. Upon initial exposure to their excitation wavelength, all channels open at once and as they proceed through their photocycles will finally reach an equilibrium (the stationary current phase) of constantly opening and closing channels, in which ∼60% of all illuminated channels are in the open-channel state,[16] inferred by the peak-to-stationary current ratios. The stationary current is very robust; the individual contribution of a single channel is small and of short persistence, because each individual channel closes quickly and reopens again. Therefore, illumination with a closing wavelength, exciting the conducting P520 or respective state, accelerating channel
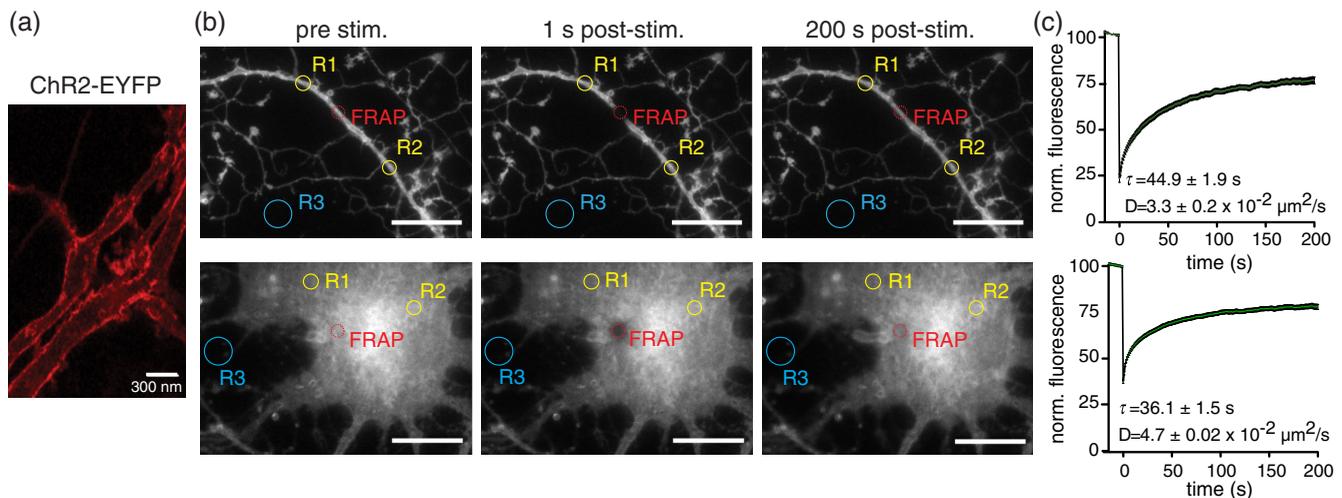
Fig. 1 Channelrhodopsin localization and diffusion in the membrane. (a) STED microscopy image of ChR2-EYFP in the dendrites of a transfected hippocampal neuron in culture. scale bar = 300 nm. (b) FRAP experiments of ChR2-EYFP in transfected neuronal processes (top) and cell bodies (bottom) before (left), immediately after (middle), and 200 s after (right) photobleaching of the indicated area. scale bars = 20 μm. R1 and R2 indicate nonbleached control regions, and R3 indicates background fluorescence black level, used for normalization of fluorescence recovery following photobleaching. (c) Quantitation of FRAP in neuronal processes (top; $n = 42$) and cell bodies (bottom; $n = 48$). Error bars indicate SEM.

closure, is thought to have only a minor influence on the total photocurrent of fast photocycle channels. As expected, photocurrents of fast photocycle variants were generally strong and disappeared quickly when illumination ceased (Fig. 2).

The most commonly used fast-photocycle channelrhodopsin variant contains the H134R mutation, which promotes enhanced stationary photocurrents.[17] This channel was activated by 405- and 488-nm light, yielding photocurrents of several hundred pA, and was not activated by wavelengths greater than 561 nm [Fig. 2(a), top]. 594-nm light was previously reported to be the most efficient wavelength to close step function ChR2 channels.[15] H134R channels activated with 488-nm light showed a small but measurable reduction in photocurrent only in response to 594-nm coillumination. The photocurrent was reduced by ∼10% or ∼20% when channels were activated with 296 or 80 mW/cm² 488 nm light, respectively [Fig. 2(a), middle]. Increasing the 594-nm laser power increased the inactivation accordingly [Fig. 2(a), bottom].

T159C mutants are reported to possess increased photocurrents.[18] Photocurrents were induced by 405- and 488-nm light (and not further redshifted wavelengths) and were indeed approximately twice as large as those of H134R channels [Fig. 2(b), top]. However, these channels showed barely perceptible inactivation with overlapping 405- or 594-nm illumination, when activated by either 488-nm light [Fig. 2(b), middle] or

405-nm light [Fig. 2(b), bottom]. Interestingly, the addition of the E123T mutation—which speeds up the photocycle and channel kinetics for temporal precision[18]—further increased peak and stationary currents to more than 1.5 nA and 700 pA, respectively, when channels were activated with 488-nm light and resulted in weak photocurrents of 250 pA when activated with 405-, 561-, and 594-nm light. This channel was inactivated slightly by 594-nm light following activation with 488-nm light [Fig. 2(c), middle]. Due to its increased activation in the red spectrum, photocurrents of E123T/T159C elicited by 405-nm light increased even further with simultaneous illumination with 561- or 594-nm light [Fig. 2(c), bottom].

The L132C ChR2 mutant also has high photocurrents and was reported to make channels calcium permeable,[19] which could be advantageous to assay focal activation by calcium imaging. This channel displayed strong photocurrents of 750 pA in response to 405-nm activation and 1.3 nA for 488-nm activation, with a reduced peak–stationary current ratio, compared to other channels. A pronounced slope in decay time indicates slow channel kinetics [Fig. 2(d), top]. However, this channel also exhibited minimal inactivation with 594-nm light following activation with 405- or 488-nm light [Fig. 2(d), bottom].

The C1V1 and ReaChR redshifted channels and the Chronos and CoChR channels also have a fast photocycle, but it has not
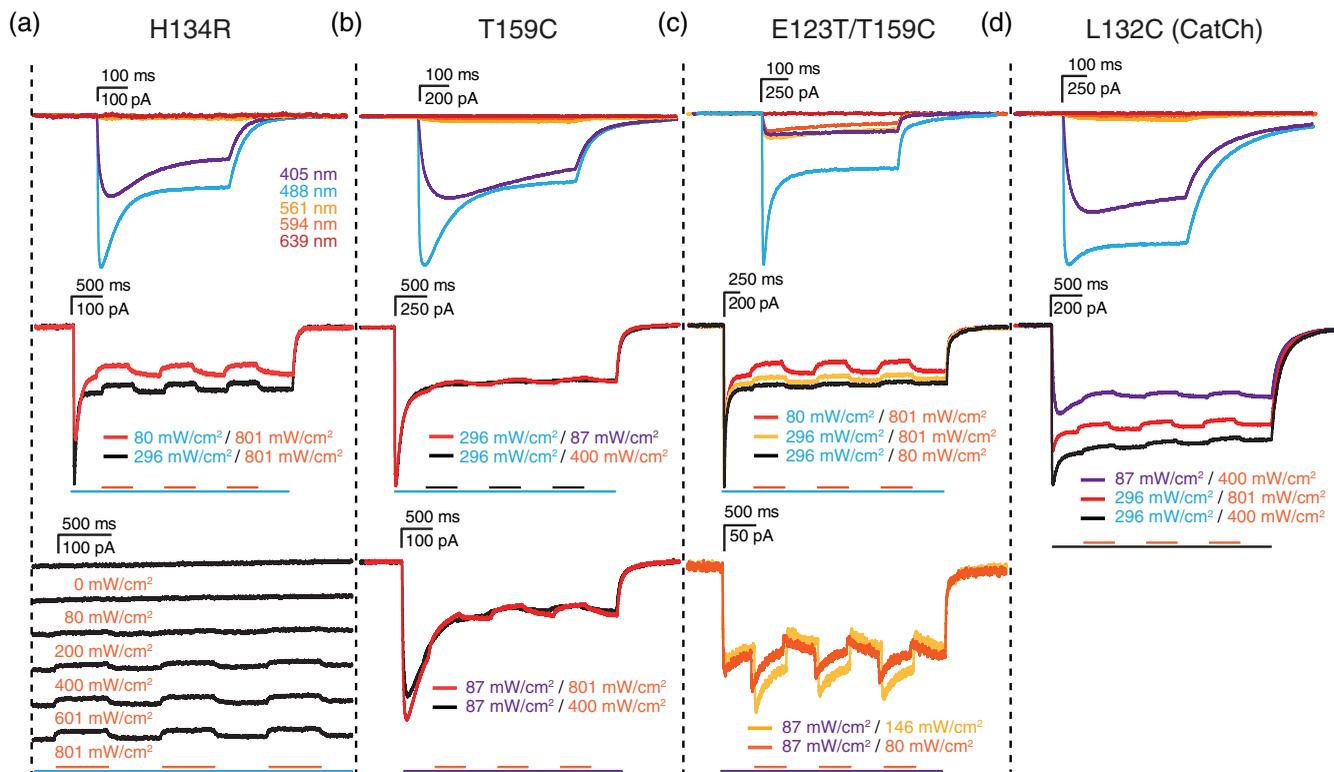
Fig. 2 Illumination evoked photocurrents of light-gated channels with fast photocycles. (a) Photocurrents from recorded hippocampal neurons in culture expressing H134R, (b) T159C, (c) E123T/T159C, and (d) L132C channels, elicited by 405, 488, 561, 594, and 639 nm single wavelength laser illumination (top panels) and by coillumination with different wavelengths (lower panels). Photocurrent recordings at specific illumination wavelengths are indicated by the respective color of the recording. Scale bars above current traces indicate recorded current (vertical) and time (horizontal). For coillumination experiments, bars below recordings indicate time of illumination for the indicated color-coded wavelength. Black bars refer to coillumination with the color of the depicted traces in cases where more than one coillumination wavelength was tested. Activating laser intensities were 405 nm, 87 mW/cm²; 488 nm, 296 mW/cm²; 561 nm, 146 mW/cm²; and 639 nm, 22 mW/cm², unless otherwise indicated.

been as extensively studied. The C1V1 channel—comprised of *Chlamydomonas* and Volvox ChR1 domains and containing the E122T/E162T mutations that speed up the photocycle[15]—and ReaChR[20] possess an extended activation spectrum toward the redshifted wavelengths, but responded almost equally well to 405- and 488-nm light and had maximal photocurrents of ~600 pA [Figs. 3(a) and 3(b)]. These channels showed little inactivation under coillumination. Photocurrents of C1V1 E122T/E162T activated with 405-nm light were actually further increased by coillumination with 488- or 561-nm light [Fig. 3(a)]. CoChR and Chronos channels[21] could be efficiently opened by illumination at 405-, 488-, and 561-nm light, where 488 nm evoked the strongest photocurrents [Figs. 3(c) and 3(d)]; CoChR in particular featured remarkably strong photocurrents

of 3 to 4 nA. CoChR photocurrents could be reduced slightly when 405-nm activation was combined with 561-nm coillumination, and when 488- or 561-nm activation was combined with 405-nm coillumination. This was particularly surprising in the case of 561-nm evoked photocurrents, because in single wavelength tests, 405-nm evoked currents were stronger than those evoked by 561-nm light [Fig. 3(c)]. 488-nm coillumination increased photocurrents of the 561-nm activated state of CoChR. Chronos only showed a weak photocurrent reduction for simultaneous 405-nm illumination, when activated with 488-nm light [Fig. 3(d)]. On the contrary (and as expected from single wavelength results), 405-, 488-, or 561-nm coillumination of Chronos transfected neurons increased photocurrents of the 405- or 561-nm activated states.
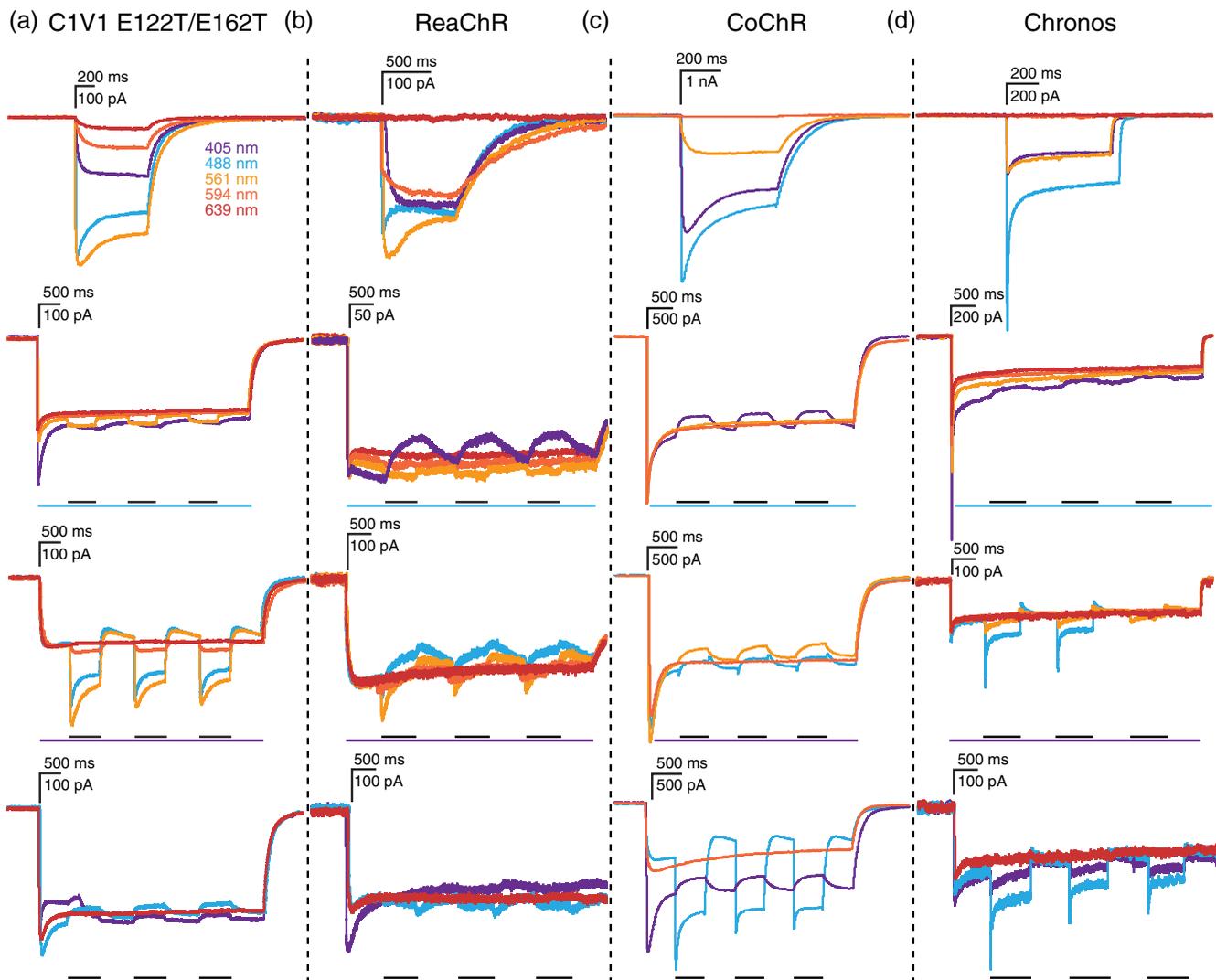

Fig. 3 Illumination evoked photocurrents of redshifted light-gated channels. (a)–(d) Photocurrents of the indicated channels elicited by 405, 488, 561, 594, and 639 nm single wavelength laser illumination (top panels) and by coillumination with different wavelengths (lower panels). Photocurrent recordings at specific illumination wavelengths are indicated by the respective color of the recording. Scale bars above individual experiments indicate recorded current (vertical) and time (horizontal). For coillumination experiments, bars below recordings indicate time of illumination for the indicated color-coded wavelength. Black bars refer to coillumination with the color of the depicted traces in cases where more than one coillumination wavelength was tested. Activating laser intensities were 405 nm, 87 mW/cm²; 488 nm, 296 mW/cm²; 561 nm, 146 mW/cm²; and 639 nm, 22 mW/cm², and inactivating laser intensities were 405 nm, 662 mW/cm²; 488 nm, 3.15 W/cm²; 561 nm, 1.33 W/cm²; 594 nm, 801 mW/cm²; and 639 nm, 283 mW/cm².

The stabilized step-function opsin (SSFO) channel variant, ChR2 C128S/D156A,[11,15,22] has properties that make it attractive for a putative nanoscale focal activation approach; it is opened by blue-light and closed by green-light. This channel has been well characterized by spectral analysis of photocurrent responses to different wavelengths and has an optimal opening wavelength of 470 and optimal closing wavelength of 590.[15] We therefore used similar wavelengths to test coillumination. In single and coillumination tests, however, we found maximal photocurrents of only 40 to 60 pA with full field activation of transfected neurons, as expected [Fig. 4(a), top]. In addition, 488-nm light-activated channels were only partially closed

with coillumination of 561 [Fig. 4(a), top] or 594 nm [Fig. 4(a), bottom] light.

In an attempt to increase the photocurrent but maintain the switching capabilities of channels, we made a ChR2 variant with C128A/H134R/T159C mutations. We reasoned that H134R would enhance stationary photocurrents,[17] T159C would increase photocurrents,[18] and C128A would allow the channel to be switched to a closed state with 561-nm illumination (and would inactivate more quickly than the C128S mutation[22]). This channel exhibited photocurrents of 350 to 400 pA in response to 405- or 488-nm illumination and weak photocurrents when illuminated at 561 nm. The photocurrent
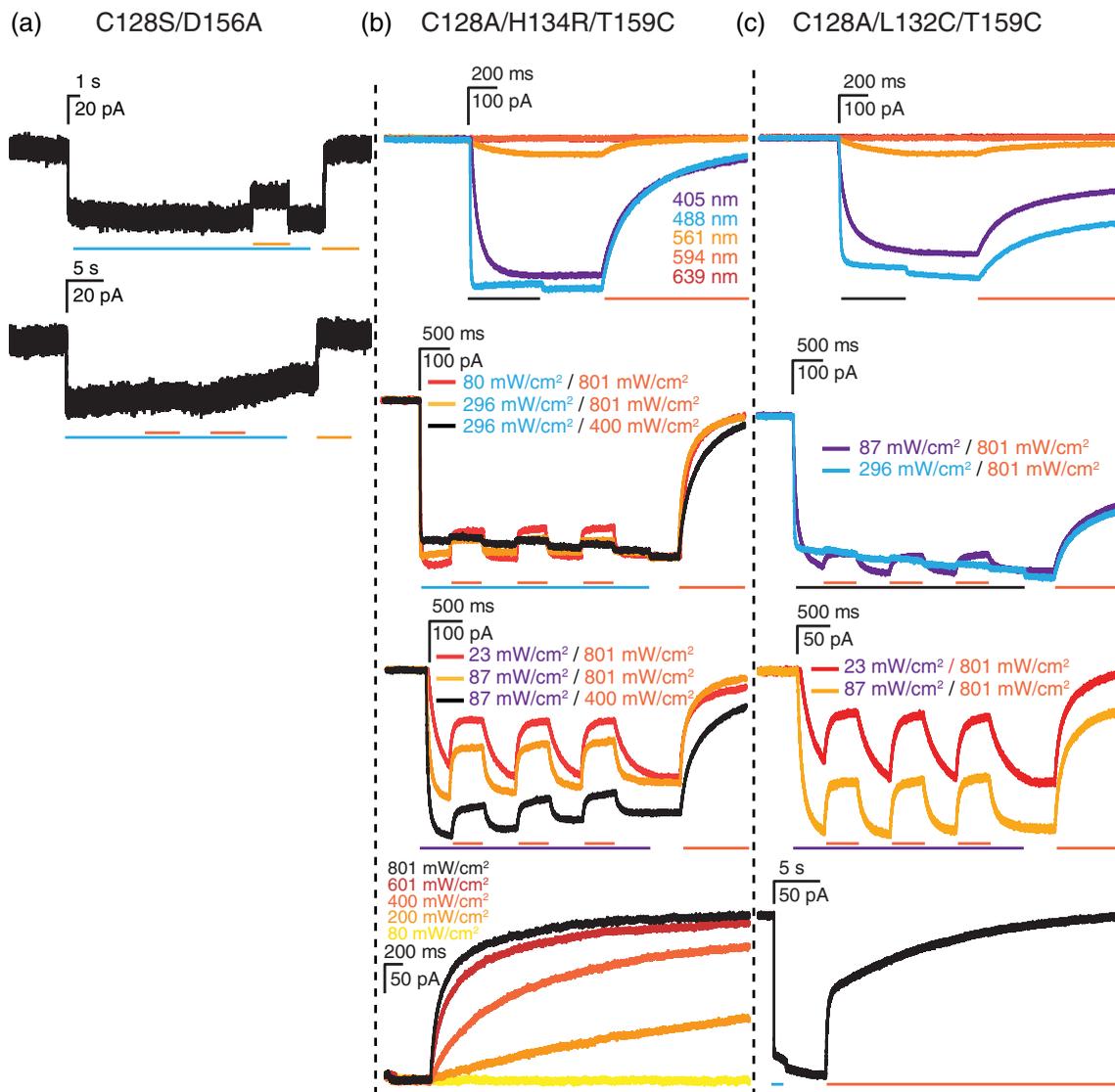
Fig. 4 Illumination evoked responses of light-gated ion-channels with slow photocycles (step-function opsins). (a) Responses to 405, 488, 561, 594, and 639 nm single wavelength laser illumination and coillumination of C128S/D156A (step-function opsin), (b) C128/H134R/T159C, and (c) C128S/L132C/T159C switchable channels. Photocurrent recordings at specific wavelength illumination are indicated by the respective color of the recording. Scale bars above individual experiments indicate current (vertical) and time (horizontal). For coillumination experiments, bars below recordings indicate time of illumination for the indicated color-coded wavelength. Black bars refer to coillumination with the color of the depicted traces in cases where more than one coillumination wavelength was tested. Activating laser intensities were 405 nm, 87 mW/cm²; 488 nm, 296 mW/cm²; 561, 146 mW/cm²; 594 nm, 80 mW/cm²; and 639 nm, 22 mW/cm², unless otherwise indicated.

was completely inactivated by single wavelength illumination with 594-nm light and partially inactivated by coillumination. This channel was inactivated even more efficiently (with 594-nm light) when activated with 405-nm light [Fig. 4(b)]. Thus, this channel appears more promising than the original SSFO channel for focal activation, in terms of larger photocurrent, and closing efficiency with inactivating light coillumination. We also generated a C128A/L132C/T159C channel, which should also have higher photocurrents and close with inactivating coillumination, and in addition be permeable to calcium, thus allowing calcium imaging to detect activation. This channel did indeed have similar high photocurrents and inactivation properties compared to the C128A/H134R/T159C channel, although its closing kinetics were slower [Fig. 4(c)].

The C1V1 E122T/C167S channel is the corresponding step function version of the C1V1 channel. This channel maintained its redshifted wavelength activation properties and was activated by 488-, 561-, and 594-nm light, and weakly by 639-nm light. The C1V1 E122T/C167S channel showed efficient photocurrent reduction when stimulated with 561-nm light and coilluminated with 405-nm light, as indicated by earlier studies;[23] channels activated by 561-nm light could be efficiently closed by 405-nm light (but not by 488-nm light) [Fig. 5(a)]. In contrast to the inactivating influence of 405-nm light on 561-nm activated currents, 405-nm coillumination following 488-nm light activation increased photocurrents further.

We further tested the addition of the switchable mutations (C108S and D136A, corresponding to C128S and D156A in ChR2) to the CoChR channel variants, which showed the largest photocurrents of all channels tested. (Chronos variants showed intracellular accumulation in neurons resulting in small photocurrents and were therefore not tested further.) The C108S mutation alone reduced the photocurrent of CoChR from ~4 nA to 150 pA for 488-nm activation and to 50 pA for 405-nm activation but did indeed cause the channel to be partially inactivated by 594-nm light, following activation with 405- or 488-nm light [Fig. 5(b)]. In addition, the CoChR C108S mutant exhibited 488-nm mediated channel closure, as seen from the photocurrent increase after stopping illumination. The addition of the D136A mutation to create CoChR C108S/D136A virtually eliminated this effect and increased 405-nm evoked photocurrents, which were inactivated to a greater extent by 594-nm light [Fig. 5(c)].

As opposed to other approaches, the eNPAC construct—which expresses ChR2 H134R and NpHR3.0, a hyperpolarizing light-gated chloride pump, at equimolar amounts via connection by a P2A site that is cleaved intracellularly—does not depend on a specific illumination to close channels but rather on a balance between blue light activation of ChR2 H134R to depolarize cells and red light activation of the NpHR3.0 proton pump to hyperpolarize cells.[2] Photocurrent responses from eNPAC-expressing neurons were detected for all tested wavelengths (Fig. 6). 405- and 488-nm evoked responses were almost identical to standard ChR2 H134R responses. However, 488-nm photocurrents displayed a small and brief transient after illumination ceased, most likely because NpHR3.0 is weakly activated by 488-nm light, and when this light is terminated the pumping of chloride-ions by NpHR3.0 stops more quickly than ChR2 H134R channels close, leading to a transient depolarization. This effect was not present for 405-nm excitation, implying that NpHR3.0 is not significantly activated by 405-nm light. When illuminated with 561- and 594-nm light, hyperpolarizing currents of

~400 pA were recorded from eNPAC-expressing cells. Because ChR2 H134R is not activated by red wavelengths, these currents are predominantly from NpHR3.0 activation.

During initial channel tests of step-function opsins, we noted that even when 801 mW/cm^2 (100%) 594-nm laser power was used, maximal channel inactivation was not reached. Therefore, we increased the 594-nm laser intensity by modifying the light path and exchanging the light guide from the DL594 laser module to the microscope with the beam splitter in the DirectFRAP unit (see Sec 4) and tested the effect of this modification on the most promising candidates inactivated by 594 nm light: ChR2 C128A/H134R/T159C and the CoChR C108S and C108S/D136 mutants (Fig. 7). ChR2 C128A/H134R/T159C channels were activated with 41.92 W/cm^2 (10%) 488-nm laser power or 9.92 W/cm^2 (20%) 405-nm laser power through the DirectFRAP laser path and inactivated by simultaneous illumination three consecutive times for 500 ms each, with 594-nm light of different intensities [Fig. 7(a)]. The photocurrent values from these three exposures were pooled and compared to the average maximum photocurrent elicited by 500-ms single 488- or 405-nm illumination (between coillumination and a final 594-nm single wavelength exposure) to calculate % photocurrent reduction by coillumination with 594-nm light [Fig. 7(b)]. In addition, activation intensities from 19.51 to 90.48 W/cm^2 (1% to 20%) were tested against 129.75 W/cm^2 (100%) DL594 power [Fig. 7(c)]. Using the modified setup, we were able to reduce photocurrents of ChR2 C128A/H134R/T159C elicited with 488-nm light by 54% and similar magnitude currents elicited with 405-nm light by 90%. Increased photocurrents were elicited by higher 488-nm activation intensities, which caused less efficient photocurrent reduction by coillumination. However, increased photocurrents elicited by higher [up to 9.92 W/cm^2 (20%)] 405-nm activation were still efficiently reduced by coillumination.

We then tested 488- and 405-nm activation of CoChR C108S and CoChR C108S/D136A channels at varying intensities with maximal 594-nm inactivation [Fig. 7(d)]. Photocurrent reduction was most efficient for 405-nm activation and 594-nm coillumination. For CoChR C108S, photocurrents were higher for 488-nm than for 405-nm light activation, and 488-nm light evoked photocurrents inactivated only slightly less efficiently than those elicited by 405-nm light. CoChR C108S/D136A, on the other hand, had slightly higher photocurrents elicited by 405-nm light than 488-nm light, which were eliminated with 594-nm coillumination, whereas 488-nm elicited photocurrents were only inactivated by ~50%. A photocurrent increase when 488-nm illumination is discontinued was visible for the CoChR channel and especially for the C108S mutant. In general, currents of the CoChR step function variants were weaker than the ChR2 step function variants and did not increase when higher 405-nm light intensities were used. However, 405-nm evoked currents could be efficiently reduced by exposure to 594-nm light. These experiments suggest that 405-nm light is the ideal activation wavelength for experiments where strong photocurrents and efficient photocurrent reduction, using 594-nm coillumination, is needed.

A summary of all channels tested in terms of activating/inactivating wavelengths, magnitude of photocurrent, and degree of inactivation is shown in Fig. 8. The fast photocycle variants H134R, T159C, E123T/T159C, L132C, C1V1 E122T/E162T, ReaChR, CoChR, and Chronos all showed only ~1% to 20% inactivation by coillumination [Fig. 8(a)]. Lowering activation
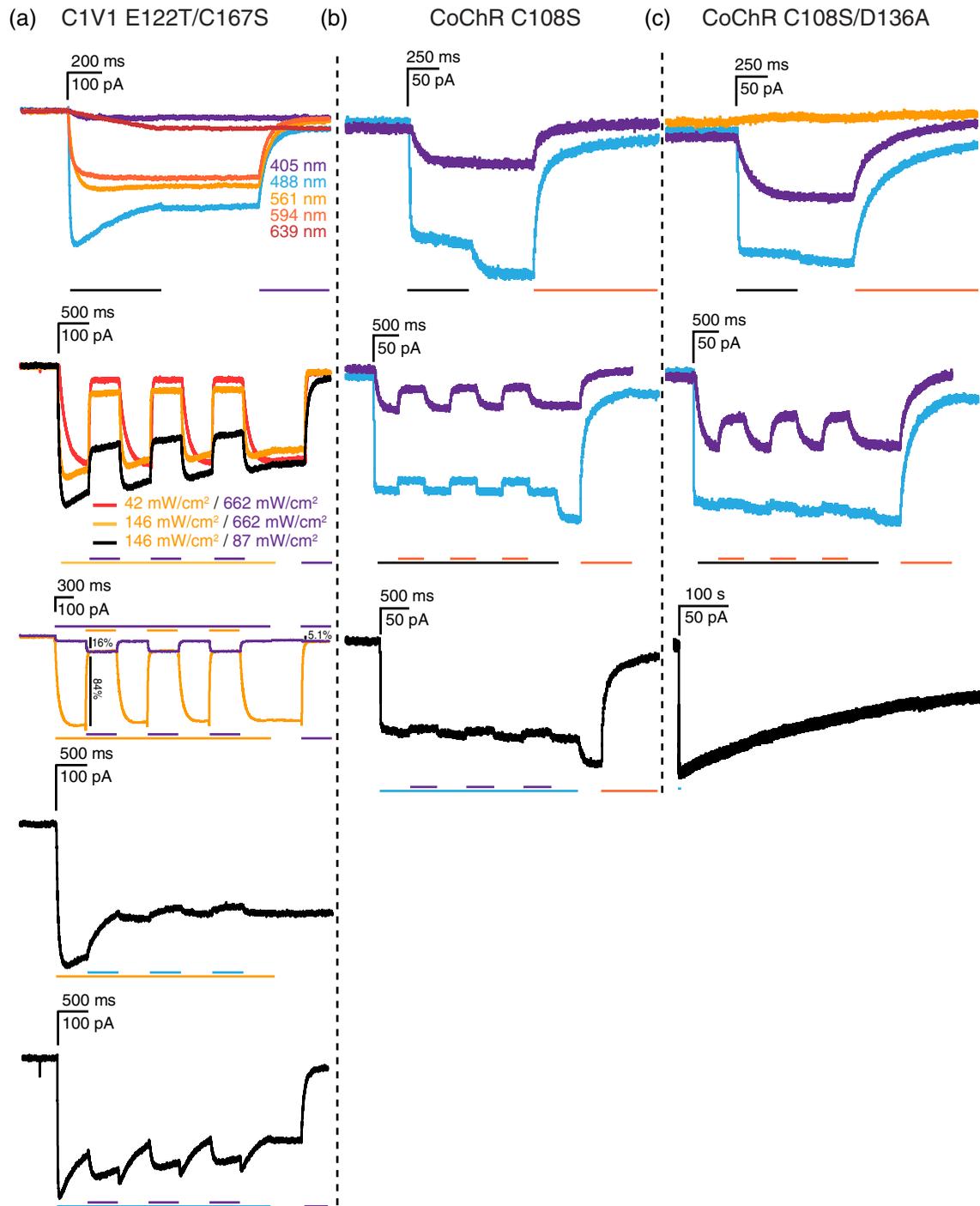
Fig. 5 Illumination evoked responses of redshifted and higher photocurrent light-gated ion-channels with step-function mutations. (a) Responses to 405, 488, 561, 594, and 639 nm single wavelength laser illumination and coillumination of (a) C1V1 E122T/C167S, (b) CoChR C108S, and (c) CoChR C108S/D136A channels. Photocurrent recordings at specific wavelength illumination are indicated by the respective color of the recording. Scale bars above individual experiments indicate current (vertical) and time (horizontal). For coillumination experiments, bars below recordings indicate time of illumination for the indicated color-coded wavelength. Black bars refer to coillumination with the color of the depicted traces in cases where more than one coillumination wavelength was tested. Activating laser intensities were 405 nm, 87 mW/cm²; 488 nm, 296 mW/cm²; 561 nm, 146 mW/cm²; 594 nm, 80 mW/cm²; and 639 nm, 22 mW/cm², and inactivating laser intensities were 405 nm, 662 mW/cm²; 488 nm, 3.15 W/cm²; 561 nm, 1.33 W/cm²; 594 nm, 801 mW/cm²; and 639 nm, 283 mW/cm², unless otherwise indicated.
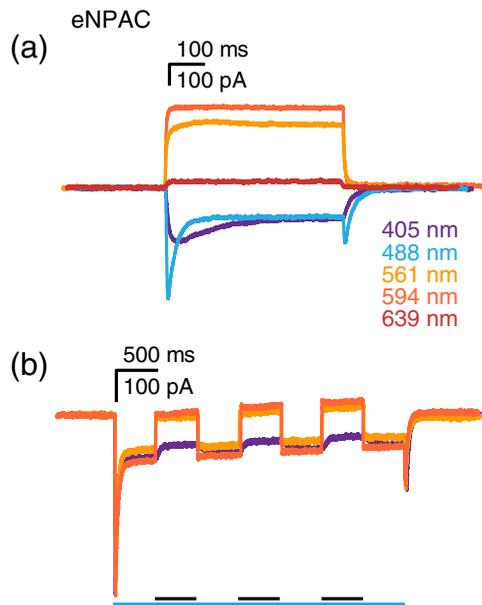
Fig. 6 Illumination evoked responses of equimolar ChR2 H134R and NpHR3.0 (eNPAC). Evoked responses of eNPAC with 405, 488, 561, 594, and 639 nm single wavelength laser (a) illumination and (b) coillumination. Scale bars above individual experiments indicate current (vertical) and time (horizontal). For coillumination experiments, bars below recordings indicate time of illumination for the indicated color-coded wavelength. Black bars refer to coillumination with the color of the depicted traces. Activating laser intensities were 405 nm, 87 mW/cm^2; 488 nm, 296 mW/cm^2; and 561 nm, 146 mW/cm^2, and inactivating 594 nm coillumination intensity was 801 mW/cm^2.

laser intensity increased the extent of inactivation, but decreased overall photocurrent. Raising inactivation laser intensity also increased the extent of inactivation, only slightly for these channel variants. The CoChR channel had two to six times higher photocurrent than other channels, with ∼15% to 20% inactivation. The original stable step-function opsin variant C128S/D156A exhibited 33% inactivation with coillumination but a photocurrent of only ∼50 pA. The addition of the C128A switchable mutation to channels with H134R/T159C or L132C/T159C mutations reduced photocurrents slightly but increased the extent of inactivation, especially by 405-nm light. The addition of the C167S switchable mutation to the C1V1 channel did not reduce the photocurrent (elicited by 561-nm light) but did increase the extent of inactivation (by 405-nm light) to ∼84%. Adding the C108S or C108S/D136A switchable mutations to CoChR significantly reduced the photocurrent, from ∼2000 to 200 pA, but improved channel inactivation. eNPAC ChR2 photocurrents were completely inactivated by coillumination to activate NpHR3.0. In further tests of the most promising candidates, e.g., C128A/H134R/T159C and CoChR C108S or C108S/D136A channels [Fig. 8(b)], we found that both the photocurrent and efficiency of inactivation plateaued. 405-nm light activation increased inactivation efficiency compared with 488-nm light. In general, photocurrent magnitude and degree of inactivation were inversely related, and both photocurrent strength and inactivation efficiency plateaued and were not further increased by increasing activation/inactivation light intensity.

To estimate the size of illuminated regions for which photocurrents can be detected, we tested focal single wavelength 488-

nm light activation of proximal neuronal processes of cells expressing the ChR2 T159C channel. Photocurrents elicited by illumination of membrane areas with diameters down to 1.2 μm could reliably be detected using electrophysiological patch-clamp recordings in the whole-cell configuration [Fig. 9(a)]. However, detectable photocurrents were already weak, suggesting that photocurrents from smaller areas will be beyond detection limits, especially for switchable channel variants, which have reduced photocurrents. We therefore first investigated the feasibility of nanoscale optogenetic stimulation using a microscale approach and an illumination strategy borrowed from super-resolution microscopy, in which a central area is illuminated with a wavelength of light that activates channelrhodopsins while an overlapping donut region is simultaneously illuminated with a wavelength of light that inactivates these channels [Fig. 9(b)], thereby confining activation to a small central region. To accomplish this, we used photoactivation masks for 405- or 488-nm illumination of 16.7-μm diameter areas, in combination with a donut-shaped 594-nm inactivation mask, resulting in a central activated region of 6.2 μm in diameter. We first verified illumination regions using a fluorescently labeled slide [Fig. 9(c)]. We then tested the approach on neurons transfected with eNPAC, a construct that coexpresses equimolar amounts of ChR2 H134R and NpHR3.0[2]. In neurons transfected with eNPAC, coillumination with 594-nm light effectively inactivated photocurrents evoked by 488-nm light [Fig. 9(d)]. Stimulation of eNPAC-expressing cells with 488-nm light in 6.2 or 16.7 μm regions resulted in ∼12 pA [Fig. 9(d), blue trace] or ∼45 pA [Fig. 9(d), black trace] steady-state photocurrents, respectively. When a 16.7-μm spot of 488-nm light stimulation of ChR2 was combined with 594-nm costimulation of NpHR3.0 in an overlapping donut (resulting in a central activated region of ∼6.2 μm), net photocurrents could be tuned to be lower [Fig. 9(d), orange trace], higher [Fig. 9(d), red trace], or equivalent to [Fig. 9(d), black trace] depolarization achieved with the 6.2-μm stimulation mask alone. Thus, NpHR3.0 currents are tunable in their strength by adjusting 594 nm laser power to counterbalance ChR2-mediated depolarization in the coilluminated area.

In a second approach, the same illumination principle was applied to the ChR2 slow-photocyle variant C128A/H134R/T159C [Fig. 9(e)]. The respective evoked photocurrents for 6.2 and 16.7 μm wide areas, illuminated with 405-nm light, were 50 and 150 pA. When 16.7 μm 405-nm photostimulation was combined with an overlapping donut of 594-nm illumination, photocurrents could be reduced to values close to those evoked by stimulation of a 6.2-μm area alone, independent of the order in which the different wavelengths were applied [Fig. 9(e)].

3 Discussion

We investigated an approach to focally confine channelrhodopsin activation using switchable light-gated channels and an illumination approach inspired by STED/RESOLFT microscopy. Of all tested candidates, the ChR2 C128A/H134R/T159C and the slow CoChR variants C108S and C108S/D136A—activated with 405-nm light and inactivated by coillumination with 594-nm light—and the C1V1 E122T/C167S channel—activated by 561-nm light and inactivated by 405-nm light—were most promising in terms of highest photocurrents and efficient inactivation with coillumination. The combination of coexpression of a depolarizing cation-channel and hyperpolarizing light-gated
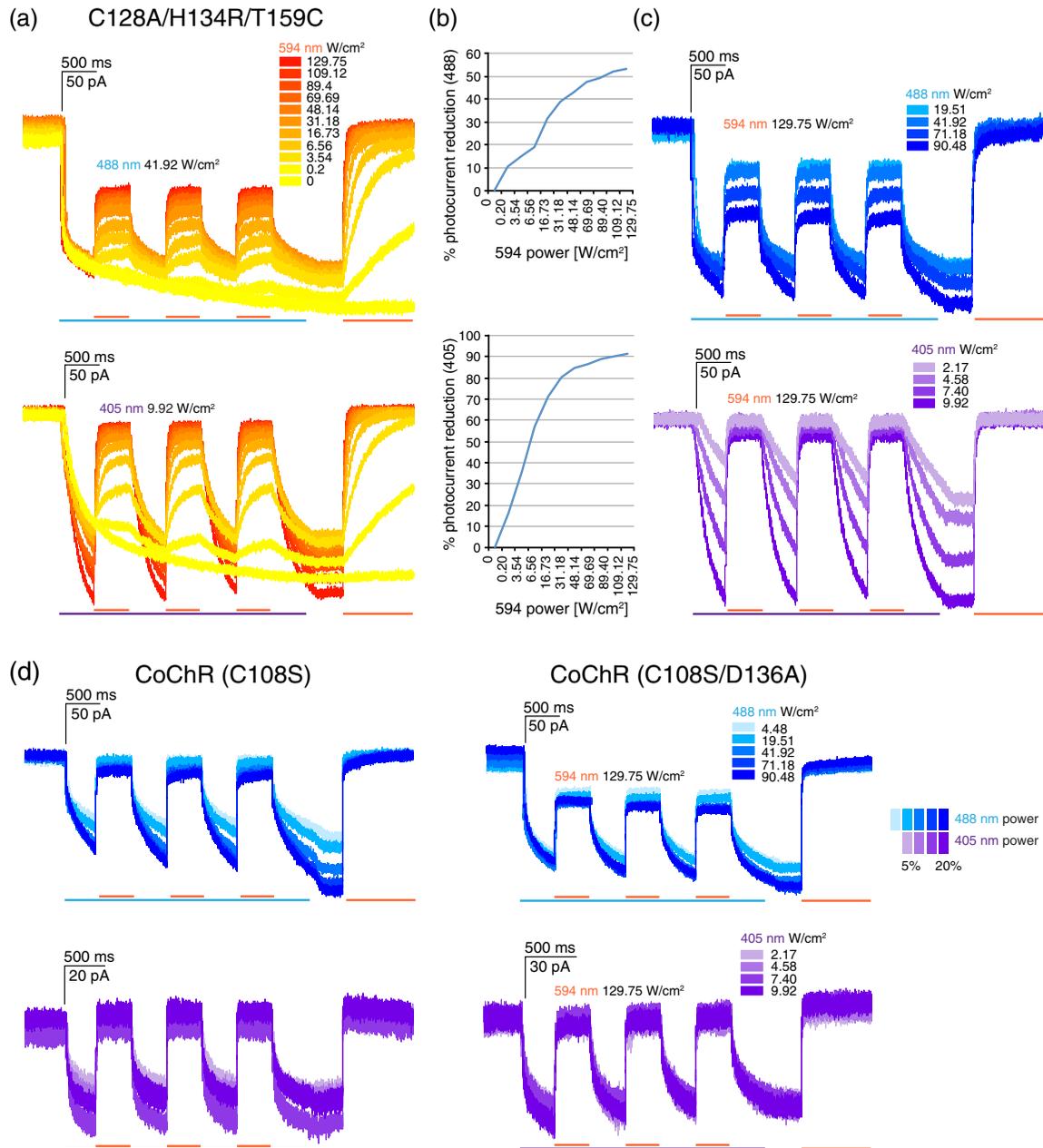
Fig. 7 Reduction of 488- and 405-nm evoked photocurrents from ChR2 C128A/H134R/T159C, CoChR C108S, and CoChR C108S/D136A channels. (a) Effect of coillumination of different 594-nm laser powers on 488 nm (top) or 405 nm (bottom) evoked currents; 594-nm laser powers are indicated in the color-coded inset and were tested in 10% steps from 0% to 100% laser power. (b) Relationship between 594-nm laser intensity and photocurrent reduction. (c) Influence of activating 488 nm (top) or 405 nm (bottom) laser power on 594 nm light-mediated photocurrent reduction. Scale bars indicate recorded currents (vertical) and time (horizontal). (d) Photocurrent reduction of 488-nm light (top) and 405-nm light (bottom) evoked currents in CoChR C108S (left) and C108S/D136A (right) mutants. Trace and stimulation bar colors represent laser wavelengths and intensities (5%, 10%, 15%, and 20%).

chloride-pump (eNPAC) also represents an interesting alternative, in which counterbalancing currents can be used to cause a net voltage change of 0 mV in the area of 405- or 488-, and 594-nm coillumination.

Based on our experiments, three approaches using light-gated ion-channels/pumps could be used to achieve focal photostimulation. The first is simultaneous activating wavelength illumination of a central region and inactivating wavelength coillumination in a donut overlapping this central activated region. The second (which could be used with step-function opsin channels that do not show sufficient inactivation during coillumination) is fast sequential illumination, in which channels are opened with one wavelength and subsequently closed in an outer donut region. For this approach, the time between initial channel opening and closing of the outer channels should be as short as possible. The third option makes use of the eNPAC construct to control depolarizing and hyperpolarizing currents with different wavelengths of light in central and
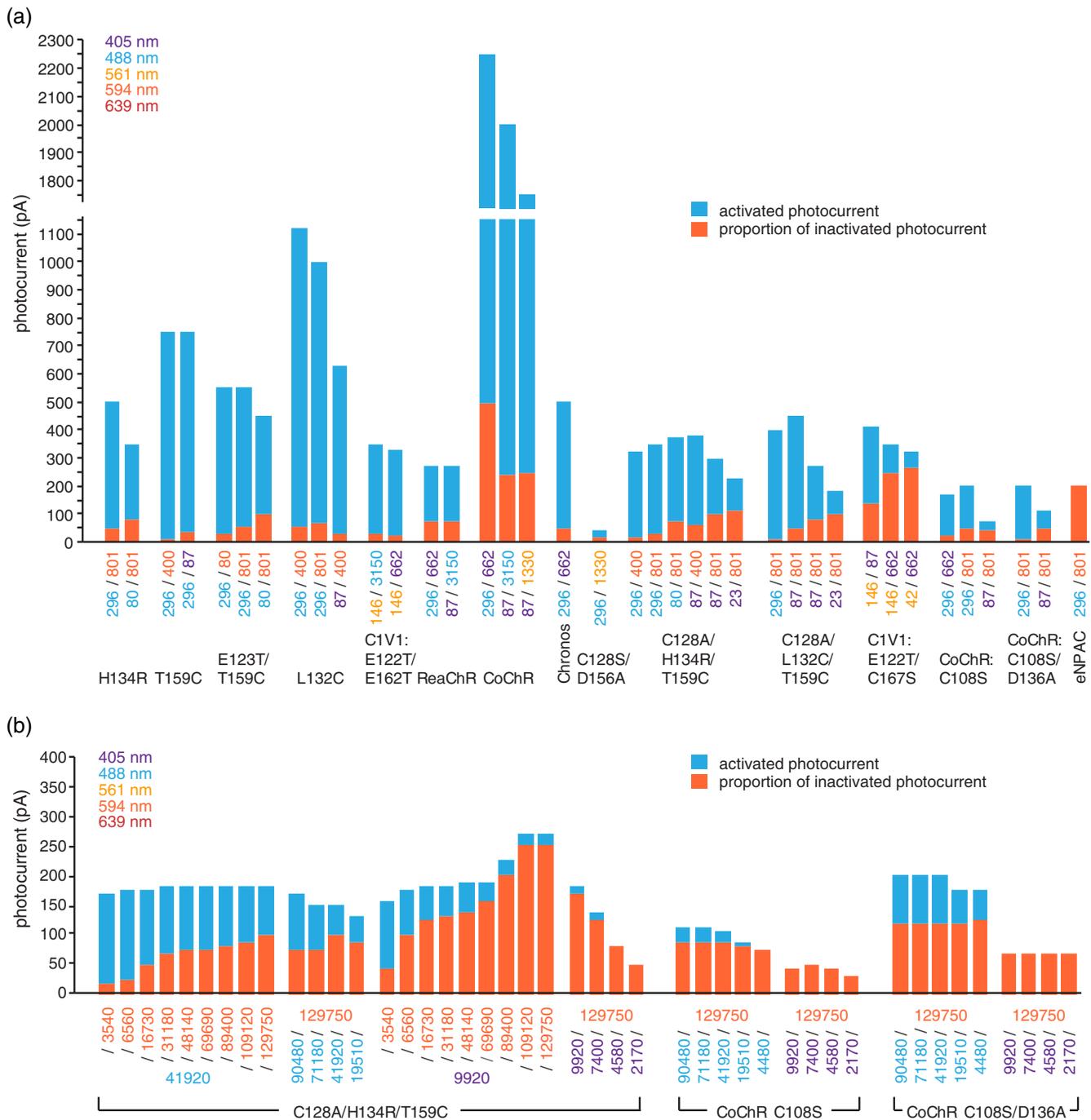
Fig. 8 Summary of activating/inactivating wavelengths, photocurrent magnitude, and degree of inactivation for all channels tested. (a) Magnitude of photocurrent (blue) and portion of photocurrent inactivated (orange) by the indicated activation/inactivation intensities (mW/cm^2) color-coded by wavelength, for all channels tested, and for selected candidates (b).

surrounding regions. Theoretically, the wavelengths can also be inverted, producing highly focal areas of hyperpolarization, mimicking inhibitory synapses. However, the use of eNPAC is not ideal for nanoscale optogenetics, since (1) coactivation of ChR2 and NpHR3.0 will reduce membrane resistance and may shunt physiological inputs, (2) simultaneous Na$^+$ and Cl$^-$ import may lead to osmotic changes in the cell (although these effects should be minimal with focal activation), (3) the efficiency of activation/inactivation may be variable given that a 1:1 stoichiometric expression of ChR2 and NpHR3.0

cannot be guaranteed, due to differences in rates of folding, trafficking, and degradation, and (4) activation/inactivation will depend on membrane voltage since ChR2 is an ion channel with reversal potential near 0 mV, and NpHR is a pump whose current depends only weakly on voltage.

Efficient inactivation of channels with coillumination usually required reducing activation laser intensities. It was reported that 594-nm inactivating light should be roughly 1000-fold more intense than 488-nm activating light to achieve photocurrent-inactivation of ∼95% for ChR2 C128S.[24] In our experiments,
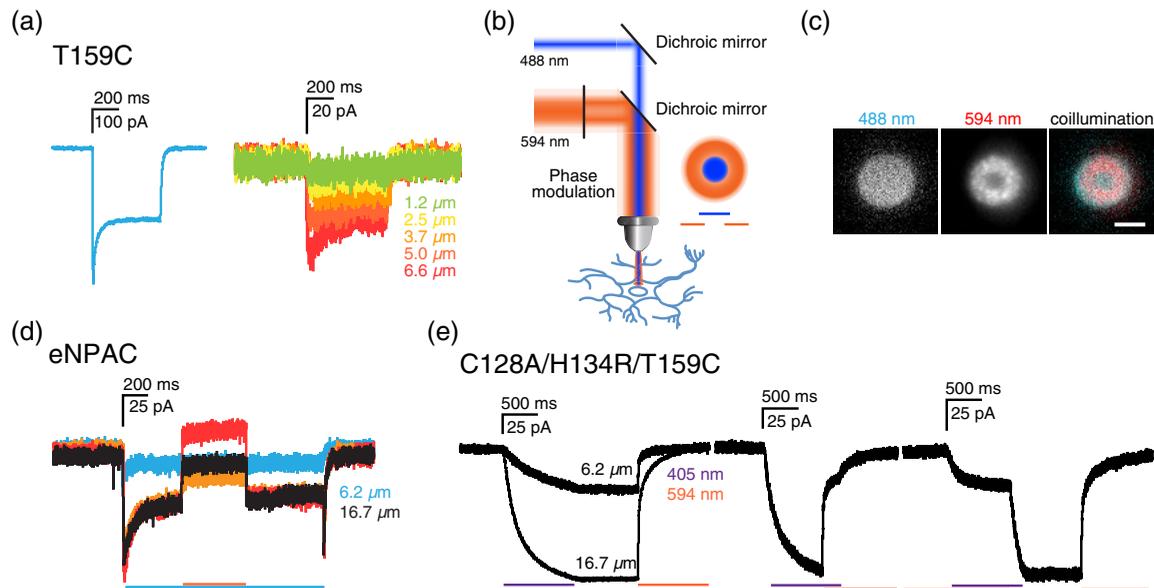
Fig. 9 Electrophysiological recordings of photocurrents in focally stimulated areas. (a) T159C channelrhodopsin photocurrents elicited by 90.48 W/cm² 488 nm full field (left) or focal (right) activation of the cell body. (b) Illumination scheme for focal activation based on STED/RESOLFT microscopy: 488-nm activation light is brought together with a 594-nm donut-shaped inactivation beam. The two wavelengths of illumination overlap and inactivate channels within the donut region, resulting in a potentially subdiffraction limited central activated region. (c) Images of yellow text highlighter, used as a dye for a uniform fluorescent field on a coverslip illuminated with 488-nm light in a 16.7-μm diameter central region, and 594-nm light in an overlapping donut region, resulting in a central activated region of 6.2 μm. scale bar = 10 μm. (d) eNPAC photocurrents elicited by 488 nm light in a focal 6.2 μm (blue) or 16.7 μm (black) diameter region, or in a 16.7-μm region combined with a 594-nm laser overlapping donut to inactivate the overlapping region resulting in a central activated region of 6.2 μm (black trace). 594-nm laser intensity can be tuned to drive NpHR3.0-mediated hyperpolarizing currents to be weaker (orange trace), stronger (red trace), or equivalent to (black trace) the photocurrent elicited by 6.2 μm stimulation of ChR2 (blue trace). (e) Photocurrents of the ChR2 C128S/H134R/T159C variant evoked by 6.2 or 16.7 μm regions of 9.92 W/cm² 405-nm laser illumination and subsequent 594-nm illumination mediated closure (left), and with coillumination of 16.7 μm 488-nm illuminated region and an overlapping donut of 594-nm illumination, resulting in a 6.2-μm central activated region (right). When a 16.7-μm 488-nm illuminated region was combined with a 594-nm overlapping donut region (leaving a central 6.2 μm region of activation), the photocurrent is reduced to a level similar to that evoked by a 6.2-μm region alone.

we tested the lowest available laser power for activation (1%; 4.48 W/cm²). The power density could be further reduced using filters or beam splitters to achieve 1000-fold higher 594-nm power densities; however, this would mainly reduce photocurrents from activated channels and not lead to a more efficient channel gating. Interestingly, channels were more efficiently inactivated by 594-nm light following 405-nm light activation, than following 488-nm light activation, even at only ~100-fold higher 594-nm light power densities. We assume that 405-nm light illumination activates the P470 open state but does so less efficiently. However, it is also possible that these channels have a separate conducting state for stimulation in the UV spectrum, which is more easily reduced by 594-nm illumination. In any case, 405-nm activation was superior to 488-nm activation, for subsequent inactivation by coilluminating 594-nm light to close channels. For eNPAC, 405-nm light evoked ChR2-mediated depolarization was completely counterbalanced by 80 to 160 mW/cm² 594-nm illumination to activate hyperpolarizing NpHR3.0. Although these values fluctuated between experiments, they were minimal, given approximate equimolar expression of ChR2 and NpHR3.0 in eNPAC. In this case, 405-nm activation light (rather than

488 nm) also avoids currents that arise from NpHR3.0 blue-light activation.

An important question is whether current optogenetic tools are powerful enough to allow detection at the nanoscale. Photocurrent recordings from *Xenopus* oocytes have yielded estimated single channel conductances of ~50 fs for wild-type ChR2, with single channel currents of ~5 fA.[25] Using nonstationary noise analysis, single channel Na⁺ conductances of wild-type ChR2 and ChR2 H134R in HEK cells were determined to be 41.5 fs at 200 mM extracellular Na⁺, with single channel currents of 3.5 fA at −60 mV.[16] Other studies using nonstationary noise analysis estimate ChR2 single channel conductance at around 1 ps, which principally would allow single channel recordings.[26] However, the absence of such published recordings to date suggest this value may be an overestimation. During the stationary current photocycle phase, ~60% of ChR2 H134R channels are expected to be in the open-channel state.[16,17] Thus, ~226 channels are active per μm² cell membrane in HEK cells.[16] If the proposed channel density in HEK cells translates to a similar presence in neuronal membranes, stimulation of a synapse size area (0.04 μm²) would lead to the opening of approximately nine channels and currents

of 31.5 to 45 fA at −60 mV—too low to be detected using standard electrophysiological methods, or currently available calcium or voltage sensors that can be imaged at wavelengths that do not influence light-gated channels.[27,28] An increase in channel abundance in the membrane, however, e.g., by higher expression levels or targeting motifs to synapses, or an increase in single channel conductance could enable detection of activation at the nanoscale. To mimic synaptic activation, ideally channels would possess properties that match currents elicited by AMPA receptors at excitatory synapses, where 1 to 2 AMPA receptors open during the peak of the postsynaptic current.[29,30] Single channel AMPA conductance is ∼8 to 10 ps.[30,31] To match currents of a single AMPA receptor, the conductance of a wild-type ChR2 would need to be enhanced roughly 200-fold. Light-gated genetically modified ionotropic glutamate channels (LiGluRs), which are based on AMPA receptors and can be activated and inactivated by two different wavelengths of light, are another alternative.[32,33] LiGluR steady-state currents were reported to be fivefold larger than those of wild-type ChR2,[34] i.e., on the order of Chronos currents, but LiGluR requires the addition of an exogenous chemical photoswitch and may also alter the native firing properties of cells in which it is expressed since it is based on the glutamate receptor that is natively present in the brain.

Although we demonstrate the feasibility of a focal optogenetics approach at the microscale, we also show that at present channel conductance is too low to allow nanoscale activation. Nevertheless, this work may be useful for future development of nanoscale optogenetics. It is likely that stronger conducting channel variants will be found. New single channel optogenetic tools with faster switching kinetics that allow depolarization and hyperpolarization could allow nanoscale activation. For instance, the ion selectivity of ChR2 has recently been selectively modified to create a chloride-conduction channel.[35,36] It would also be interesting to test the sdChR C138S/E154A variant, because it has been reported to possess good photocurrent inhibition.[24] In addition, optogenetics now extends beyond light-gated channels. Inducing protein conformational changes or interactions in nanodomains by light, for example, may be feasible using this technique.

4 Materials and Methods

4.1 Animals

Use of animals for experimentation was approved and performed according to the specifications of the Institutional Animal Care and Ethics Committees of Goettingen University (T10.31) and of the German animal welfare laws.

4.2 Mammalian Expression Constructs

Vectors for CaMKIIα-controlled expression of channelrhodopsins (pAAV-CaMKIIα-hChR2-mCherry/EYFP-WPRE) including the H134R, T159C, E123T/T159C, and C128S/D156A ChR2 variants,[15,18] ChR1 VChR1 chimera C1V1 E122T/E162T,[37] and the eNpHR3.0-EYFP (halorhodopsin) and hChR2(H134R)-mCherry fusion construct eNPAC (pAAV-hsyn-eNPAC)[2] are available from Karl Deisseroth (Stanford University/Howard Hughes Medical Institute). The L132C channelrhodopsin (CatCh) variant[19] was provided by Ernst Bamberg (Max-Planck-Institute for Biophysics, Germany). With the assistance of GenScript, pAAV-CaMKIIα-hChR2

(H134R)-mCherry-WPRE, pAAV-CaMKIIα-hChR2(T159C)-mCherry-WPRE, and pAAV-CaMKIIα-C1V1(E122T/E162T)-TS-mCherry were mutated to combine common ChR characteristics and yield the slow-photocycle switchable high-conducting variants hChR2(C128A/H134R/T159C), hChR2(C128A/L132C/T159C), and C1V1(E122T/C167S) in the same backbone. Additional ChRs selected for their strong photocurrents, Chronos and CoChR, together with their mutated slow-photocycle switchable variants, Chronos C145S and C145S/E162T and CoChR C108S and C108S/D136A, under CMV promotor control are available from Edward Boyden (Massachusetts Institute of Technology).

4.3 Dissociated Primary Hippocampal Cultures

Dissociated hippocampal cultures were cultured on 25-mm coverslips (Paul Marienfeld GmbH; cat. no. 0117650) coated with 0.04% polyethylenimine (PEI) (Sigma; cat. no. P3143) in six-well plates (CytoOne; cat. no. CC7672-7506); 2 ml of 0.04% PEI in dH_2O, stored at −20°C was added per well at room temperature for ∼14 h, followed by three washes with dH_2O after which plates were directly used for cultures or stored in dH_2O at 4°C until needed.

The hippocampal culture method was adapted from Gary Banker.[38,39] Pregnant Wistar rats were euthanized between E18 and E19 by CO_2. Embryos were extracted and brains transferred to 10 cm dishes containing dissection medium (Hank's Balanced Salt Solution + 10 mM HEPES). Hemispheres were separated, meninges removed, and hippocampi extracted and collected in a 15-ml falcon-tube containing dissection medium on ice. Tissue was digested in 2-ml 0.25% trypsin-EDTA (Gibco; cat. no. 25200-056) for 20 min at 37°C, washed three times with 5-ml dissection medium, triturated in 1-ml plating medium (Dulbecco's modified eagle medium with 10% FBS; Gibco), and filtered through a 100-μm cell strainer (Corning, Inc.; cat. no. 352360). Cell yield was determined using trypan blue staining (Sigma; cat. no. T8154), and cells plated at densities of 30,500 to 37,000 cells/cm^2 per coverslip and cultured at 37°C and 5% CO_2. The following day plating medium was exchanged for 2 ml culture medium [Neurobasal with 1X B-27 supplement, 1× glutamax and penicillin (5000 U/ml)/streptomycin (5000 μg/ml); all from Gibco]. 5 μM AraC was added once on DIV7.

4.4 Calcium Phosphate Transfection

On DIV3, conditioned culture medium was collected and exchanged for pre-equilibrated (37°C and 5% CO_2) Opti–MEM (Gibco; cat. no. 11058–021). One-third fresh culture medium was added to the collected conditioned medium that was filtered through a 0.22-μm syringe-driven filter (Millipore; cat. No. SLGV033RS), and stored in the incubator. For each well of a six-well plate, 7.5-μl 2 M $CaCl_2$ and 3.5 to 4 μg plasmid DNA in 60-μl dH_2O were mixed and 60-μl transfection buffer (274 mM NaCl, 10 mM KCl, 1.4 mM Na_2HPO_4, 15 mM glucose, 42 mM Hepes, pH 7.05 to 7.12) was then added dropwise, under gentle agitation. This solution was incubated for 20 min at room temperature and then gently added to cells, which were returned to the incubator for 90 min. The Opti-MEM plus transfection mix was then exchanged for 37°C and 10% CO_2 pre-equilibrated neurobasal medium, returned to the incubator for 10 min, and subsequently exchanged for the stored conditioned medium.

4.5 STED Imaging

Hippocampal neurons transfected with ChR2-EYFP were imaged using a custom-built STED microscope. Excitation pulses of 490 nm wavelength were delivered using a pulsed-laser diode (Toptica Photonics, Graefelfing, Germany), followed by pulses at 595 nm delivered by a Ti:Sapphire laser (MaiTai; Spectra-Physics, Darmstadt, Germany) for stimulated depletion with a donut-shaped focal profile created by introducing a polymeric phase plate (RPC Photonics, Rochester, New York) into the path of the STED beam. The STED and excitation pulse beams were synchronized by external triggering, overlapped with a custom-made dichroic mirror, and focused into a 1.3-NA objective lens (PL APO, CORR CS, 63×, Leica, Wetzlar, Germany). Fluorescence was passed through a 535/50 band-pass filter and collected with an optical fiber connected to an avalanche photodiode (PerkinElmer, Waltham, Massachusetts). Images were recorded with resonant mirror scanning along the x-axis and stage scanning along the y-axis at 10 μs pixel dwell times.

4.6 FRAP Experiments

Transfected hippocampal neurons at DIV12 growing on coverslips were transferred into a low-profile RC–41LP imaging chamber (Warner Instruments; cat. no. 64-0368) filled with 1-ml extracellular solution (in mM: 145.4 NaCl, 5 KCl, 2 CaCl$_2$, 1 MgCl$_2$, 10 HEPES, 7 glucose in dH$_2$O; 300 mOsm, pH 7.4). Live imaging was conducted on a Zeiss Axio Observer.Z1 microscope equipped with a 405-nm 50-mW diode laser, 488-nm 100-mW OPSL, 561-nm 40-mW diode laser, and 639-nm 30-mW diode laser, a TIRF slider module, a laser manipulation DirectFRAP module, and an Evolve 512 EMCCD camera (Photometrics). Image acquisition was controlled with AxioVision 4.8.2 software (Zeiss). Images were collected using a 100× objective [alpha Plan-Apochromat 100×/1.46 oil DIC (UV) Vis-IR] and laser intensities of 10% and 1 s intervals with a gain of 800 and exposure times below 1 s. Following stable baseline acquisition for at least 10 s, defined regions of cell bodies and processes were bleached for 1 s with 100% 488-nm laser intensity using the laser manipulation with DirectFRAP tool and photoactivation mask with 2.5 μm diameter. Average intensities were recorded from the FRAP region and three additional regions of interest: two different control regions on the cell and one off the cell to detect background noise. Background noise was subtracted, signal from control areas were used to compensate for bleaching, and data were normalized by setting the average of fluorescence values from 1 to 10 s before bleaching at 100%. Tau (τ) was computed for bleach recovery curves fit with a single exponential curve using Prism v5.0d software (GraphPad).

4.7 Electrophysiology and Optogenetics

Electrophysiological recordings were made from DIV8-DIV12 hippocampal neurons transfected with light-gated channels/pumps on DIV3. Cultures were transferred to a custom-made imaging chamber, adapted to fit with the motorized stage, in extracellular solution (in mM: 148 NaCl, 2.4 KCl, 2 CaCl$_2$, 1 MgCl$_2$, 10 HEPES, 7 glucose in dH$_2$O; 300 mOsm, pH 7.4). To isolate ChR2 photocurrents and block spontaneous network activity, 1 μM TTX (Alomone Labs; cat. no. T–550), 50 μm APV (Abcam; cat. no. ab120003), 10 μM CNQX (Sigma; cat. no. C239), and 10 μm gabazine (Abcam; cat. no. ab120042) were added to the extracellular solution. Patch pipettes with 3 to 5 MΩ resistance were made from fire polished borosilicate capillaries (Harvard Apparatus; cat. no. 300060, OD 1.5 mm × ID 0.86 mm) with a P–97 Micropipette Puller (Sutter Instruments). Silver wire electrodes were chlorinated with a 2 M KCl solution using an ACl-01 apparatus (npi electronic). Patch pipettes were backfilled with 7-μl internal solution (in mM: 130 potassium gluconate, 8 KCl, 2 CaCl$_2$, 1 MgCl$_2$, 10 EGTA, 10 HEPES, 2 Mg-ATP, 0.3 GTP-Na; 290 to 295 mOsm, pH 7.3), using 20 μl microloader pipette tips (eppendorf; cat. no. 5242 956.003). A pipette holder was controlled using a MPC-385-2 micromanipulator system (Sutter Instruments). Whole-cell patch-clamp recordings were obtained with an EPC10 USB double patch-clamp amplifier and Patchmaster software (HEKA) at 25 kHz sampling intervals.

All optogenetic experiments were conducted on an inverted Zeiss Axio Observer.Z1 microscope equipped with a 405-nm 50-mW diode laser, 488-nm 100-mW OPSL, 561-nm 40-mW diode laser, and 639-nm 30-mW diode laser, 20× LD A-Plan, 40× and 63× EC Plan-NEOFLUAR and 100× α Plan-APOCHROMAT objectives, a TIRF slider module, a laser manipulation DirectFRAP module, and an Evolve 512 EMCCD camera (Photometrics). An additional 594-nm 100-mW DPSS laser (Rapp OptoElectronic GmbH; Hamburg, Germany) was added to the epifluorescence light path with a 940-μm light guide, together with custom photomasks, complementing the existing DirectFRAP photomasks by adding a 594-nm border (2 μm for 100× objective) around the DirectFRAP photomasks. A photomask of a 150-μm wide area or no photomask was used for initial single wavelength full-field illumination tests. All lasers were operated by TTL pulses delivered by the HEKA amplifier.

Laser powers were determined with a laser power meter (Fieldmate) and a silicon OP-2 VIS optical sensor (Coherent GmbH; Dieburg, Germany) at the back aperture of the 40× and 100× objectives, using two aluminum masks to represent the respective exit pupil diameter, 10.7 and 4.8 mm. There was no difference in the measured power between those two masks. Laser intensities were measured after 4 to 6 h of use and with the TIRF/FRAP beamsplitter set at 50% TIRF/50% FRAP. The measured laser powers were subsequently corrected for the respective transmission of the objective. Laser output generally fluctuated ±30 μW and the measurement error was previously determined to be ∼10%. 594 nm laser intensity was measured using the 200-μm light guide and respective powers for the 100-μm light guide were extrapolated. For initial tests of light-gated channel candidates, we used wide-field illumination with the 40× objective at power densities of 405 nm 87 mW/cm^2, 488 nm 296 mW/cm^2, 561 nm 146 mW/cm^2, and 594 nm 801 mW/cm^2 or 1.08 W/cm^2. In experiments in which the light path was adjusted to increase 594-nm laser power (by exchanging the 940-μm light guide for a 100-μm light guide, and the DirectFRAP beamsplitter for an AHF beam splitter), power densities using the 40× objective were 405 nm 27 to 65 mW/cm^2, 488 nm 228 mW/cm^2, 561 nm 133 mW/cm^2, and 594 nm 129.75 W/cm^2 or 267 W/cm^2. Because the 594-nm photomasks did not cover the whole wide-field illuminated area, FRAP photomasks of similar area were used for stimulation of 405-nm light at 9.92 W/cm^2 and 488 nm light at 41.92 W/cm^2.

Because channels with a stable open state are sensitive to broad-spectrum daylight conditions, channels were closed

before and after each experiment by a brief illumination with the respective closing wavelength. Channelrhodopsins were characterized by their responses to 500-ms light pulses of 405, 488, 561, 594, and 639 nm, using the DL594 laser and no photomask for the 594 nm and the TIRF laser for the other wavelengths. To test focal optogenetic stimulation and record responses, 488-nm light pulses were delivered using DirectFRAP photomasks and the 100× objective; 594-nm Rapp Opto custom-designed photomasks were overlaid to produce a coillumination donut surrounding a central region.

Microscope and components including lasers were controlled with Zeiss AxioVision and Zen Blue software. Transfected cells were identified by fluorescence and selected based on health and membrane integrity. Recordings were acquired from cells voltage-clamped at −70 mV. Liquid junction potential, pipette, and cell capacitance influences were compensated. Recordings were managed with IGOR Pro (Wavemetrics; version 6.22A) and the Patcher's Power Tools extension for HEKA files provided by the Department of Membrane Biophysics at the Max Planck Institute for Biophysical Chemistry in Goettingen. In cases where small shifts in timing of laser pulses occurred, traces were manually aligned to illumination onset for comparison.

Disclosures

Acknowledgments

References

1. K. Deisseroth, "Optogenetics," *Nat. Methods* **8**(1), 26–29 (2011).
2. V. Gradinaru et al., "Molecular and cellular approaches for diversifying and extending optogenetics," *Cell* **141**(1), 154–165 (2010).
3. L. A. Gunaydin et al., "Ultrafast optogenetic control," *Nat. Neurosci.* **13**(3), 387–392 (2010).
4. D. Brinks et al., "Painting with rainbows: patterning light in space, time, and wavelength for multiphoton optogenetic sensing and control," *Acc. Chem. Res.* **49**(11), 2518–2526 (2016).
5. T. Schikorski and C. F. Stevens, "Quantitative ultrastructural analysis of hippocampal excitatory synapses," *J. Neurosci.* **17**(15), 5858–5867 (1997).
6. Y. P. Zhang and T. G. Oertner, "Optical induction of synaptic plasticity using a light-sensitive channel," *Nat. Methods* **4**(2), 139–141 (2007).
7. P. Schoenenberger et al., "Optimizing the spatial resolution of channelrhodopsin-2 activation," *Brain Cell Biol.* **36**(1–4), 119–127 (2008).
8. S. K. Mohanty et al., "In-depth activation of channelrhodopsin 2-sensitized excitable cells with high spatial resolution using two-photon excitation with a near-infrared laser microbeam," *Biophys. J.* **95**(8), 3916–3926 (2008).
9. A. M. Packer et al., "Two-photon optogenetics of dendritic spines and neural circuits," *Nat. Methods* **9**(12), 1202–1205 (2012).
10. E. Papagiakoumou et al., "Scanless two-photon excitation of channelrhodopsin-2," *Nat. Methods* **7**(10), 848–854 (2010).
11. C. Bamann et al., "Structural guidance of the photocycle of channelrhodopsin-2 by an interhelical hydrogen bond," *Biochemistry* **49**(2), 267–278 (2010).
12. C. Bamann et al., "Spectral characteristics of the photocycle of channelrhodopsin-2 and its implication for channel function," *J. Mol. Biol.* **375**(3), 686–694 (2008).
13. K. Nikolic et al., "Photocycles of channelrhodopsin-2," *Photochem. Photobiol.* **85**(1), 400–411 (2009).
14. K. Stehfest et al., "The branched photocycle of the slow-cycling channelrhodopsin-2 mutant C128T," *J. Mol. Biol.* **398**(5), 690–702 (2010).
15. O. Yizhar et al., "Neocortical excitation/inhibition balance in information processing and social dysfunction," *Nature* **477**(7363), 171–178 (2011).
16. K. Feldbauer et al., "Channelrhodopsin-2 is a leaky proton pump," *Proc. Natl. Acad. Sci. U. S. A.* **106**(30), 12317–12322 (2009).
17. G. Nagel et al., "Light activation of channelrhodopsin-2 in excitable cells of Caenorhabditis elegans triggers rapid behavioral responses," *Curr. Biol.* **15**(24), 2279–2284 (2005).
18. A. Berndt et al., "High-efficiency channelrhodopsins for fast neuronal stimulation at low light levels," *Proc. Natl. Acad. Sci. U. S. A.* **108**(18), 7595–7600 (2011).
19. S. Kleinlogel et al., "Ultra light-sensitive and fast neuronal activation with the Ca^{2+}-permeable channelrhodopsin CatCh," *Nat. Neurosci.* **14**(4), 513–518 (2011).
20. J. Y. Lin et al., "ReaChR: a red-shifted variant of channelrhodopsin enables deep transcranial optogenetic excitation," *Nat. Neurosci.* **16**, 1499–1508 (2013).
21. N. C. Klapoetke et al., "Independent optical excitation of distinct neural populations," *Nat. Methods* **11**(3), 338–346 (2014).
22. A. Berndt et al., "Bi-stable neural state switches," *Nat. Neurosci.* **12**(2), 229–234 (2009).
23. M. Prigge et al., "Color-tuned channelrhodopsins for multiwavelength optogenetics," *J. Biol. Chem.* **287**(38), 31804–31812 (2012).
24. V. Venkatachalam and A. E. Cohen, "Imaging GFP-based reporters in neurons with multiwavelength optogenetic control," *Biophys. J.* **107**(7), 1554–1563 (2014).
25. G. Nagel et al., "Channelrhodopsin-2, a directly light-gated cation-selective membrane channel," *Proc. Natl. Acad. Sci. U. S. A.* **100**(24), 13940–13945 (2003).
26. J. Y. Lin et al., "Characterization of engineered channelrhodopsin variants with improved properties and kinetics," *Biophys. J.* **96**(5), 1803–1814 (2009).
27. H. Dana et al., "Sensitive red protein calcium indicators for imaging neural activity," *Elife* **5**, e12727 (2016).
28. D. R. Hochbaum et al., "All-optical electrophysiology in mammalian neurons using engineered microbial rhodopsins," *Nat. Methods* **11**(8), 825–833 (2014).
29. E. A. Nimchinsky et al., "The number of glutamate receptors opened by synaptic stimulation in single hippocampal spines," *J. Neurosci.* **24**(8), 2054–2064 (2004).
30. N. Spruston, P. Jonas, and B. Sakmann, "Dendritic glutamate receptor channels in rat hippocampal CA3 and CA1 pyramidal neurons," *J. Physiol.* **482**(Pt. 2), 325–352 (1995).
31. P. Jonas and B. Sakmann, "Glutamate receptor channels in isolated patches from CA1 and CA3 pyramidal cells of rat hippocampal slices," *J. Physiol.* **455**, 143–171 (1992).
32. S. Berlin et al., "A family of photoswitchable NMDA receptors," *Elife* **5**, e12040 (2016).
33. M. Volgraf et al., "Allosteric control of an ionotropic glutamate receptor with an optical switch," *Nat. Chem. Biol.* **2**(1), 47–52 (2006).

34. S. Szobota et al., "Remote control of neuronal activity with a light-gated glutamate receptor," *Neuron* **54**(4), 535–545 (2007).
35. A. Berndt et al., "Structure-guided transformation of channelrhodopsin into a light-activated chloride channel," *Science* **344**(6182), 420–424 (2014).
36. J. Wietek et al., "Conversion of channelrhodopsin into a light-gated chloride channel," *Science* **344**(6182), 409–412 (2014).
37. K. Erbguth et al., "Bimodal activation of different neuron classes with the spectrally red-shifted channelrhodopsin chimera C1V1 in Caenorhabditis elegans," *PLoS One* **7**(10), e46827 (2012).
38. K. Goslin and G. Banker, "Rat hippocampal neurons in low density cultures," in *Culturing Nerve Cells*, G. Banker and K. Goslin, Eds., pp. 339–370, MIT Press, Cambridge, Massachusetts (1991).
39. S. Kaech and G. Banker, "Culturing hippocampal neurons," *Nat. Protoc.* **1**(5), 2406–2415 (2006).

Markus A. Stahlberg received his bachelor's degree from the University of Heidelberg, and his master's and PhD degree, in 2016, from the European Neuroscience Institute in Goettingen, Germany. He is currently a postdoc at the European Neuroscience Institute in Goettingen, Germany. His current research interests include visualizing mechanisms of neurotrophin transfer between cells, and optogenetic control of synapse formation.

Charu Ramakrishnan received her master's degree in zoology in 1985 and MPhil degree in molecular biology in 1987, both from Savitribai Phule Pune University. She has been research assistant and lab manager of the Deisseroth lab at Stanford University for 11 years. She is an expert in molecular biology and her current research interests are in discovering new opsins and enhancing existing optogenetic tools.

Katrin I. Willig received her PhD from the University of Heidelberg in 2006. Following a postdoc in the lab of Stefan Hell at the Max Planck Institute of Biophysical Chemistry in Goettingen, she has been a group leader with the Center for Nanoscale Microscopy and Molecular Physiology of the Brain Cluster of Excellence in Goettingen since 2014. Her current research interests include nanoscale imaging of dendritic spine dynamics *in vivo*.

Edward S. Boyden received bachelor's degrees in physics and electrical engineering and computer science from the Massachusetts Institute of Technology, and his PhD in neuroscience from Stanford University in 2005. He is currently a professor at the Massachusetts Institute of Technology and has been selected to join the Howard Hughes Medical Institute as an investigator. He is known for pioneering neurotechnologies including optogenetics and expansion microscopy.

Karl Deisseroth received his bachelor's degree from Harvard University, and MD/PhD degree from Stanford University in 1998. He is currently a professor, attending physician, and Howard Hughes Medical Institute investigator at Stanford University. He is best known for pioneering the fields of optogenetics and hydrogel-tissue chemistry.

Camin Dean received her PhD from the University of California, Berkeley, in 2003. Following a postdoc at the University of Wisconsin-Madison, she has been group leader of the Trans-synaptic Signaling Group at the European Neuroscience Institute in Goettingen, Germany, since 2010. Her current research interests include molecular mechanisms of synaptic plasticity underlying learning, remembering, and forgetting.